PCCP

Application of Electrochemical Surface Plasmon Resonance (ESPR) to the Study of Electroactive Microbial Biofilms

Journal:	*Physical Chemistry Chemical Physics*
Manuscript ID	CP-ART-06-2018-003898.R1
Article Type:	Paper
Date Submitted by the Author:	24-Aug-2018

Complete List of Authors:	Golden, Joel; US Naval Research Laboratory, Center for Bio/Molecular Science and Engineering Yates, Matthew; U.S. Naval Research Laboratory Halsted, Michelle ; University of Tennessee, Bredesen Center for Interdisciplinary Research and Graduate Education Tender, Leonard; Naval Research Laboratory,

Application of Electrochemical Surface Plasmon Resonance (ESPR) to the Study of Electroactive Microbial Biofilms

Joel Golden[1], Matthew D. Yates[1], Michelle Halsted[2], Leonard Tender[1]*
[1]Center for Bio/Molecular Science and Engineering, Naval Research Laboratory, Washington DC, 20375
[2] The Bredesen Center for Interdisciplinary Research and Graduate Education, The University of Tennessee, Knoxville, TN, 37996
*Tender@nrl.navy.mil

Abstract

Electrochemical surface plasmon resonance (ESPR) monitors faradaic processes optically by the change in refractive index that occurs with a change in redox state at the electrode surface. Here we apply ESPR to investigate the anode-grown *Geobacter sulfurreducens* biofilm (GSB), a model system used to study electroactive microbial biofilms (EABFs) which perform electrochemical reactions using electrodes as metabolic electron acceptors or donors. A substantial body of evidence indicates that electron transfer reactions among hemes of *c*-type cytochromes (*c*-Cyt) play major roles in the extracellular electron transfer (EET) pathways that connect intracellular metabolic processes of cells in an EABF to the electrode surface. The results reported here reveal that when the potential of the electrode is changed from relatively oxidizing (0.40 V vs. SHE) to reducing (-0.55 V vs. SHE) and then back to oxidizing, 70% of *c*-Cyt residing closest to the biofilm/electrode (within hundreds of nm from the electrode surface) appear to remain trapped in the reduced state, requiring as long as 12 hours to be re-oxidized. *c*-Cyt storing electrons cannot contribute to EET, yet turnover current resulting from cellular oxidation of acetate coupled with EET to the electrode surface is unaffected. This suggests that a relatively small fraction of *c*-Cyt residing closest to the biofilm/electrode interface is involved in EET while the majority store electrons. The results also reveal that biomass density at the biofilm/electrode interface increases rapidly during lag phase, reaching its maximum value at the onset of exponential biofilm growth when turnover current begins to rapidly increase.

Introduction

Electroactive biofilms (EABFs) act as electrode catalysts due to their electrode-coupled metabolism whereby a non-corrosive potentiostatically-regulated electrode serves as the metabolic electron acceptor or donor.[1-8] Central to their catalytic properties are the endogenous extracellular electron transport (EET) pathways constituent electroactive microorganisms (EMs) use to electrically connect electron consuming or generating intracellular metabolic processes with the underlying electrode surface. Not strictly catalysts,[9] EMs conserve a portion of the electron energy for growth and maintenance, and in doing so can remain active indefinitely, unlike

inorganic or *ex vivo* enzyme electrode catalysts which degrade over time. Synthetic biology offers the promise of enhancing catalytic properties of innate EM, and transforming non-electroactive microorganisms that perform desired redox reactions into EM by genetic engineering of EET pathways.[10] Envisioned applications of EABF-facilitated electrode reactions include power generation from oxidation of organic matter (electrogenesis) in raw waste streams (e.g., sewage) and sediments [11-14]; and fixing CO_2 into multi-carbon organic compounds (electrosynthesis) for use as fuels using renewable sources of electricity as a means to mitigate the impact of anthropogenic carbon emission on global climate change.[8, 15-20]

Achieving applications of EABFs at worthwhile scales requires a high-level understanding of the underlying processes. To this end, electrochemical methods have been primarily used to investigate EET of EABFs. These include chronoamperometry to characterize the rate of growth and maximum sustained rate of electrode-dependent metabolic activity [21]; cyclic voltammetry (CV)[22] to determine the underlying general mechanism of catalysis (e.g., Nernst-Monod model[23-26]); potential-step[27] and temperature-dependent electrochemical gating measurements[8, 28-32] to determine properties of long-distance (multi-cell-length) EET (LD-EET) that occur through some EABFs (i.e., redox conductivity)[27, 29, 31, 33] and to determine if heterogeneous EET (H-EET) across the biofilm/electrode interface is rate limiting[27, 29]; and electrochemical impedance spectroscopy (EIS)[34-35] which can provide information on all of the above.

There is a small but growing body of literature wherein spectroscopic methods are combined with electrochemical methods which provide deeper insights into the mechanisms of EET. Examples include absorbance spectroscopy,[36-38] which established that the oxidation state of *c*-Cyt in electrode-grown *G. sulfurreducens* biofilms is dependent on the electrode potential in a manner consistent with the role of electron-transfer reactions among *c*-Cyt in LD-EET; Raman microscopy[33, 38-43] which further indicated the role of *c*-Cyt in LD-EET of GSB and in mixed community anode-grown EABFs enriched in *Geobacter spp*. as well as a possible role of iron-sulfur clusters in EET of a cathode-grown mixed community electroautotrophic EABF[8]; florescence spectroscopy,[44] which provided evidence that the multiple non-Nernstian peaks in non-turnover voltammetry of mixed community anode-grown EABFs enriched in *Geobacter spp*. (also observed for GSB) may reflect a *c*-Cyt involved in H-EET that undergoes an electrode potential-dependent structural change; and most recently differential electrochemical mass spectrometry,[45] which enabled real-time tracking of the electrode potential-dependent rate of CO_2 generation by a mixed community anode-grown EABF enriched in *Geobacter spp*., suggesting that acetate oxidation, which requires EET to the electrode, still persists at a relatively reducing electrode potential (-0.30 V vs. SHE).

To these combined spectroscopic-electrochemical methods we add electrochemical surface plasmon resonance (ESPR).[46] ESPR is based on surface plasmon resonance (SPR), an optical method that is highly sensitive

to changes in refractive index that occur with compositional changes at the interface between a medium (e.g., an aqueous medium) and a conductive surface.[47-48 49] SPR is typically used to study adsorption[50] and other molecular-level interactions, such as antibody-antigen binding when one (antibody or antigen) is immobilized on the surface and the other binds to it.[51] The key feature of SPR is its short depth of sensitivity, which drops off exponentially within 10s to 100s of nanometers from the surface depending on the specific configuration,[47] resulting in high signal-to-noise measurements of interfacial processes. ln ESPR, the conducting surface is simultaneously used as a working electrode, enabling optical monitoring of electrochemical reactions via the change in the interfacial refractive index that occurs with the change in oxidation state of redox molecules at the electrode surface.[46, 52] This has been established for diffusing redox molecules[46] as well as electrode-bound redox molecules,[46, 53] including redox polymer-wired enzyme films[54] and electrode-bound cytochromes[55-56] – the latter two prompting the work reported on here due to the prevalent role of cytochromes in EET of EABFs including electron transfer across the biofilm/electrode interface[8, 23, 28-29, 38-40, 57-61] as well as similar electrochemical properties of redox polymer-wired enzyme films and EABFs.[23]

Here we demonstrate the use of ESPR for the first time to study an EABF, specifically GSB. Changes in the optical signal intensity is taken here to reflect the sum of 1) changes in biomass density at the biofilm/electrode interface associated with GSB growth at a fixed electrode potential (0.5 V vs SHE), and 2) changes in oxidation state of *c*-Cyt at the biofilm/electrode interface that occur during CV (between 0.40 and -0.55 V vs. SHE). The results reveal that during lag phase, when current due to EET is negligible, biomass density at the biofilm/electrode interface increases rapidly, reaching a maximum value at the onset of exponential biofilm growth when current due to EET begins to rapidly increase.[39] Changes in the SPR (optical) signal intensity observed during CV indicate that at all stages of biofilm growth, as the potential of the electrode is changed from relatively oxidizing to reducing and then back to oxidizing, approximately 70% of the ESPR detectable *c*-Cyt appear to remain trapped in the reduced state, requiring as long as 12 hours to become re-oxidized. This appears to have no effect on EET as judged by turnover current that is the same before and after CV. This result highlights the dual role of *c*-Cyt in EET and electron storage.[62] Consequently, only a relatively small fraction of *c*-Cyt nearest to the biofilm/electrode interface appear to be involved in or are required for EET to sustain the respiration needs of a fully-grown stationary phase GSB.

Methods

See Golden et al., 2015[63] for a detailed description of the SPR system used here. Briefly, a commercial surface plasmon resonance imager (SPRimager Horizon, GWC Technologies: Kretschmann configuration, 800 ± 6 nm, manually adjustable fixed angle, CCD detector) was equipped with a chamber to grow anaerobic biofilms. The

chamber, a 30 ml batch reactor, was designed and fabricated in-house out of poly(methyl methacrylate) (PMMA). The bottom of the chamber consisted of a replaceable gold-coated commercial SPR substrate (GWC Technologies) comprised of a SF10 glass slide (25 × 38 × 1 mm) onto which a 7-nm thick titanium adhesion layer was deposited followed by a 38 nm gold layer. The gold surface faced into the chamber and served as the working electrode. Before use, each substrate was vigorously rinsed with ethanol followed by sterile DI water and then air-dried. An electrical connection was made directly to the gold surface near one end of the slide using a low-temperature soldering iron and indium solder to minimize heat damage to the gold layer. The wired connection was coated with 5-min epoxy (Devcon) for strain relief. A 0.2-cm diameter (0.0314 cm^2) circular electrode was created in the center of the gold surface by masking the gold surface with biomedical adhesive tape (ARseal 90880, Adhesives Research, Inc.). We have found that masking the SPR substrate to a relatively small electrode area to chamber volume ratio minimizes mass transport limitations in the relatively small unstirred chamber, resulting in textbook voltammetry. The hole was precision-cut using a laser cutter (Mini/Helix 8000 Laser System, Epilog Laser). See supplemental materials for image of masked SPR substrate and GSB voltammetry. The chamber was sealed to the SPR substrate with a 2-cm diameter nitrile rubber O-ring. The O-ring was sealed directly against the gold surface and not the mask. The additional exposed gold area contributed to current and for this reason current and not current density is reported. The electrical connection to the gold surface was outside the chamber. The top of the chamber was sealed with a PMMA cover and included openings for a counter (¼"-diameter graphite rod), and reference electrodes (Ag/AgCl, 3 M KCl, Bioanalytical Systems) and a sparge cannula for maintaining anaerobic conditions (20:80 CO_2:N_2). The bottom of the SPR slide was mounted directly on the prism of the SPR imager using index matching fluid (Cargille Master Calibration Liquid, no. 19268, n = 1.6304). The entire SPR system and growth chamber were operated within a large incubator at 30^oC.

The surface plasmon resonance imager spatially maps, with high sensitivity, changes in refractive index due to processes occurring within the evanescent field that extends 10s to 100s of nanometers from the electrode surface. Incident light reflected off the underside of the gold layer (through the underlying glass and prism) is imaged by a CCD detector, and results in a spatial image of the light intensity reflected by the interface.[46, 52, 64-65] Spatial variation in intensity is determined by spatial variation in refractive index at the interface which occurs, for example, from non-uniform adsorption onto the SPR substrate or use of patterned molecular capture elements. In the images, brighter regions (higher SPR signal intensity) correspond to a higher refractive index, while darker regions correspond to lower refractive index. Biomass (proteins, bacterial cells, biofilms, etc.) possesses a higher refractive index than water.[50, 66-67] As such, an increase in SPR intensity is taken here in to indicate and increase in biomass density at the biofilm/electrode interface. Electrochemical activity also affects SPR intensity[46], as well as temperature.[48] For the specific SPR imager used here, SPR intensity correlates linearly with CCD pixel intensity for

intensity values between 75 and 185 (maximum range of 0−255, 8 bits). The SPR angle was set within this range before each experiment. When the intensity exceeds 180, the correlation is still positive, but linearity is lost, yielding progressively smaller increases in pixel intensity with increasing index of refraction until the SPR intensity is saturated. In cases where biofilm growth caused pixel values to exceed this range, the SPR angle was reset to be within the linear range, reducing sensitivity to changes in the interfacial refractive index.

Sequential SPR images were recorded over time to acquire spatiotemporal changes in the interfacial refractive index during biofilm growth. Images were captured at 20 s intervals during the growth experiments. The instantaneous SPR intensity depicted in Fig. 1 and Fig. 2 as a function of time and applied potential is the average SPR pixel intensity of the exposed 2-mm diameter gold electrode at each instance using ImageJ.

The SPR chamber was equipped with an electrochemical reference electrode and a counter electrode, enabling simultaneous electrochemical studies utilizing the SPR substrate as the working electrode. The working electrode was set to 0.30 V vs. Ag/AgCl during growth except when performing cyclic voltammetry (CV). CV was performed every 12 hours whereby the potential of the gold substrate was swept from 0.2 to -0.75 and back to 0.2 V (vs Ag/AgCl) at 1 mV/s, twice. All voltammetric experiments were performed with a software controlled potentiostat (Gamry 1000E, Gamry Instruments Inc.). See supplemental materials for depiction of ESPR for a reversible soluble redox molecule (ferrocenemethanol) verifying the ability to perform ESPR by methods described above.

Established procedures were used to grow *Geobacter sulfurreducens* biofilms (for example see Yates et al., 2017[1], Yates et al. (2016)[28] or Phan et al. (2016)[68]). Briefly, *G. sulfurreducens* colonies were grown on 1.5% minimum media (NB: nutrient broth) agar plates containing acetate (20 mM), fumarate (40 mM), trypticase peptone (1 g/L) and cysteine (1 mM) and incubated in an anaerobic chamber. Colonies were then picked and placed into sterile, anaerobic NB medium (g/L: 0.38 KCl, 0.2 NH_4Cl, 0.069 $NaH_2PO_4{\cdot}H2O$, 0.04 $CaCl_2{\cdot}2H_2O$, 0.2 $MgSO_4{\cdot}7H_2O$, 2 $NaHCO_3$; 10 ml/L trace minerals; final pH 6.8) containing acetate (20 mM) and fumarate (40 mM) and incubated at 30°C for two days until the OD600 reached ca. 0.5. The SPR chamber was then inoculated with 3 ml (10% inoculum) of the cultured medium. The medium used in the reactor was the same as the culture medium except fumarate was excluded, and 10 mM acetate was added.

Results

Biomass density at the GSB/electrode interface.

Biomass density at the GSB/electrode interface, indicated by SPR signal intensity, increases rapidly during lag phase (period of biofilm growth following inoculation marked by low current). It reaches a maximum value at when current due to acetate oxidation, coupled with EET to the electrode surface (poised at 0.50 V vs SHE), begins

to rapidly increase (Fig. 1, and Fig. S7 in supplemental material for biological replicates). The simultaneously recorded current (Fig. 1) exhibits the characteristic stages of GSB biofilm growth.[61] Here, SPR intensity (CCD detector pixel intensity) indicates the intensity of light (800 nm) reflected by the gold electrode. The balance of incident light is absorbed by excitation of a surface plasmon along the biofilm/electrode interface and not by *c*-Cyt, which absorb between 350 and 600 nm.[36-37] Plasmon excitation is dependent on the interfacial refractive index, which increases with increasing biomass density at the biofilm/electrode interface, resulting in an increasing SPR intensity as observed here. For the specific ESPR experiment depicted in Fig. 1, the incident angle was adjusted 4 days after inoculation in order to maintain a linear response to changes in refractive index, which occurs for SPR intensities between 75 and 185 for the specific instrumentation used here (no attempt was made to limit biofilm growth so as to remain in the linear response region without changing the incident angle). As such, the decrease in SPR intensity that occurs after the angle change suggests that a relatively large decrease in biomass density at the biofilm/electrode interface occurred during exponential growth. For comparison, in biological replicates in which the angle was not changed (Fig. S7), SPR intensity rises as in Fig. 1, converging to a fixed value by the onset of exponential growth. In those measurements however, the SPR intensity increased well beyond the linear response range and may not have been responsive to a subsequent decrease in interfacial biomass density. Regardless, in all cases the SPR intensity rose during lag phase reaching its maximum value by the onset of exponentially rising current. A control in which the inoculum contained heat-killed dead cells (55 °C for 4 hours) induced a mitigated response (Fig. S4), indicating that the SPR response observed in Fig. 1 can be primarily attributed to biological activity of cells at the electrode surface (e.g., adhesion). The SPR response observed here is consistent with that observed for the initial period of growth of *E. coli* biofilms monitored by SPR,[69] in which an initial rise in SPR intensity was attributed to displacement of water by cell replication at the interface. The response is also consistent with previous results indicating that during lag phase, GSB growth proceeds by cell replication resulting in formation of tight-packed single-cell thick domains that expand across the electrode surface before the onset of exponentially rising current at which time multiple cell layers begin to form.[39]

Abiotic ESPR voltammetry

Fig. 2 depicts a sequence of ESPR cyclic voltammograms (CVs) recorded at different stages of growth for the same GSB depicted in Fig. 1 where the potential dependency of current is consistent with CV recorded during biofilm growth[25] (see Fig. S2 for the same data as well as biological replicates in which current and SPR signal intensity are plotted vs. potential). Fig. 2a was recorded just prior to inoculation and is attributed to reduction of trace oxygen in the SPR chamber. Two CVs were recorded consecutively and the magnitude of the cathodic

current during the second CV is lower than the first, consistent with oxygen depletion during the first CV resulting in reduced mass transport of oxygen to the electrode during the second CV. The SPR signal intensity tracks both the potential and current as expected for an electrochemical reaction.[46, 52-53, 64, 70-71] Most notable is that the SPR intensity observed at the beginning of the first CV and the end of the second CV are nearly the same, indicating that performing the CVs had no lasting effect on composition or redox state of the interface. In addition, the minimum SPR signal intensity observed toward the middle of each anodic scan are the same and lags behind the current minima, emphasizing that in the case of a mass transfer-limited electrochemical reaction (the case here), current is dependent on the concentration gradient of the redox species (oxygen) at the electrode surface, which is expected to reach a maximum value then decrease during CV due to depletion of the redox species near the electrode surface[72]; whereas SPR signal intensity is dependent on the concentrations of oxidized and reduced forms of the redox species at the electrode surface which tend toward limiting values.[46]

Biotic ESPR Voltammetry

Fig. 2b depicts two turnover CVs consecutively recorded during lag phase 12 hours after inoculation for which it is assumed that residual oxygen was mostly drawn down by cells in the chamber. Here current and SPR intensity are attributed to the nascent GSB biofilm. Unlike Fig. 2a, the current minima of the consecutive CVs are the same indicating no depletion effects (consistent with excess acetate) in the medium. While the SPR intensity decreases with a decreasing anodic current, the SPR intensity minima of the second CV is lower than the first, and SPR intensity is significantly lower at the end of the second CV than at the start of the first CV. We have observed that it takes as long as 12 hours for the SPR intensity to recover to its initial value just before CVs were performed (Fig. 3). In contrast, current recovers almost immediately (Fig. 3). The same trends are observed at early exponential phase (Fig. 2c), at mid exponential phase (Fig. 2d), and at stationary phase (Fig. 2e). Fig. 2f depicts the same trend in which SPR intensity at the end of the second CV is significantly lower for the stationary phase GSB depicted in Fig. 2e, but under non-turnover condition (acetate-free medium) where the suppression in SPR signal intensity is more pronounced.

DISCUSSION

It is established that *c*-Cyt of GSB play a central role in EET including electron transfer across the biofilm/electrode interface[42,43] and that *c*-Cyt oxidation state is linked to the electrode potential in a near-Nernstian manner centered on the turnover CV midpoint potential.[23-24, 26, 36-37] It is also established that the change in the oxidation state of an electrode-bound cytochrome during CV (*sans* biofilm) can be monitored by SPR where the SPR signal is fully reversible (i.e., the cytochrome is not trapped in either oxidation state beyond a

fraction of a second).[56, 64] We therefore contend that the decrease and increase in SPR signal intensity centered on the CV current midpoint potential for each cathodic and anodic scan depicted in Fig. 2b-f, result from reduction and oxidation of *c*-Cyt at the biofilm/electrode interface in response to the changing electrode potential. Moreover, we contend that the overall downward trend in SPR signal intensity from the beginning to the end of the two sequential CVs results from storing electrons (i.e., rectification)[73] by a portion of *c*-Cyt at the interface that persist in the reduced form. To be involved in EET, *c*-Cyt must convert rapidly between the oxidized and reduced forms[29]. We also contend therefore that *c*-Cyt involved in storing electrons are not involved in EET because they are not immediately re-oxidized during the anodic scans and because the magnitude of turnover/non-turnover current is the same just before and after performing the CVs.

Following Shan, et al. (2010)[46], SPR signal intensity associated with a redox molecule is a linear sum of contributions attributed to the oxidized and reduced forms. For the SPR measurements reported here, the incident angle was fixed such that the SPR signal correlates linearly for CCD pixel intensity between 75 and 185. As such, for each growth phase depicted in Fig 2., assuming that *c*-Cyt at the biofilm/electrode surface are fully oxidized at the beginning of the first CV for which the SPR signal is greatest, and fully reduced when the SPR signal is at its lowest value during the second CV, the fraction of *c*-Cyt in the oxidized state changes linearly with the change in SPR signal between the maximum and minimum values. Since the SPR signal intensity only recovers by approximately 30% by the end of the second CV at each stage of growth, approximately 70% of *c*-Cyt detected by SPR are trapped in the reduced state under turnover condition at each stage of growth. Under non-turnover condition, approximately 95% of *c*-Cyt are trapped in the reduced state. If *c*-Cyt at the cathodic peak of the second CV are not fully reduced, then the fraction of *c*-Cyt involved in electron storage is even greater. Taken together, the results depicted in Fig. 2 suggest that beginning soon after inoculation, the majority of ESPR detectable *c*-Cyt (those residing within 100 nanometers from the electrode surface) store electrons rather than participate in EET. The stored electrons may originate from the backflow of low-potential electrons from the electrode when at a sufficiently low potential. Both turnover and non-turnover CV of GSB exhibit non-negligible cathodic current at low potentials and there is precedence for GSB to use an electrode as an electron donor[74]. Alternatively, the stored electrons may be high potential electrons resulting from persistent acetate oxidation, where the electrode cannot accept high potential electrons when it is at a low potential. In addition to the abiotic CVs (Fig. 2a), which did not exhibit a net decrease in SPR intensity, we also performed ESPR of ferrocenemethanol (Fig. S3) using the same instrumentation. Here too, the SPR intensity at the start and end of two consecutive CVs was the same, indicating that the observed decrease in SPR intensity for GSB is not an artifact of our instrumentation. Moreover, it is established that the SPR signal intensity of electrode-bound cytochromes[56, 64] does not change appreciably between the start and end of CVs, indicating that the effect observed here is not a generic cytochrome effect.

We cannot rule out that the slow relaxation of the SPR signal reflects persistent structural changes that occur at the biofilm/electrode interface and are induced by a low electrode potential. Such changes could result, for example, by electrostatic repulsion among reduced *c*-Cyt accumulating at the interface. Surface enhanced resonance Raman spectroscopy (SERRS) however revealed that for a mixed community EABF enriched from wastewater (generally a reliable source of Geobacter spp.) exhibited Geobacter-esque voltammetric features[42], as much as 90% of *c*-Cyt residing within 7 nm of the electrode surface remain reduced regardless of the electrode potential for at least 18 seconds. The slow relaxation we observe here however was not considered in that study.

Conclusions

It is established that GSB accumulates electrons in *c*-Cyt toward the outer surface of the biofilm.[33, 36-37, 40] The results reported here suggest that electrons may also accumulate in *c*-Cyt right at the electrode surface requiring as long as 12 hours to be discharged. This may have escaped previous detection by Raman microscopy[33, 39-40] and absorbance spectroscopy.[36-37] While these methods are highly sensitive to *c*-Cyt oxidation state, they lack the high sensitivity of ESPR to processes localized at the electrode surface. As such, while *c*-Cyt involved in electron storage may dominate the biofilm/electrode interface, they may comprise a tiny fraction of total *c*-Cyt associated with the biofilm.

Conflicts of interest

There are no conflicts to declare.

Acknowledgements

This was work supported by NRL base funds and by the Applied Research for the Advancement of S&T Priorities (ARAP) Program Proposal: Joint Services Laboratories' Capabilities in Synthetic Biology for Military Environments (SBME). Student research (MH) was sponsored by the Office of Naval Research NREIP program.

Figures

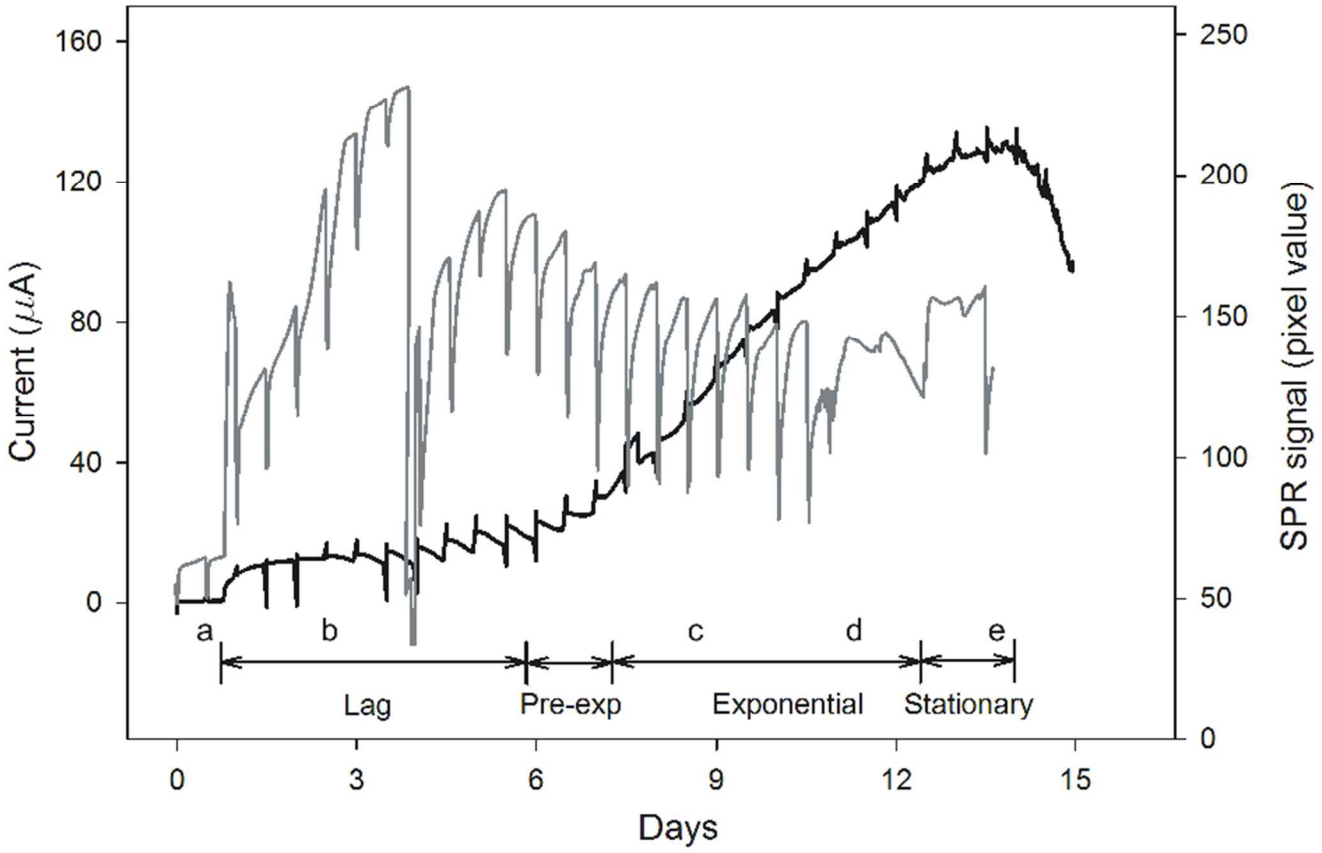

Figure 1. ESPR recorded during GSB growth while maintaining the electrode at 0.30 V vs. Ag/AgCl (0.50 V vs. SHE), turnover current (black) and SPR signal (gray). Spikes due to recording CV every 12 h. At 4 days the SPR incident angle was reset. Biofilm growth states indicated above vertical axis. See supplemental materials for biological replicates. Letters a-e indicate time when CVs depicted in Fig. 2 were recorded.

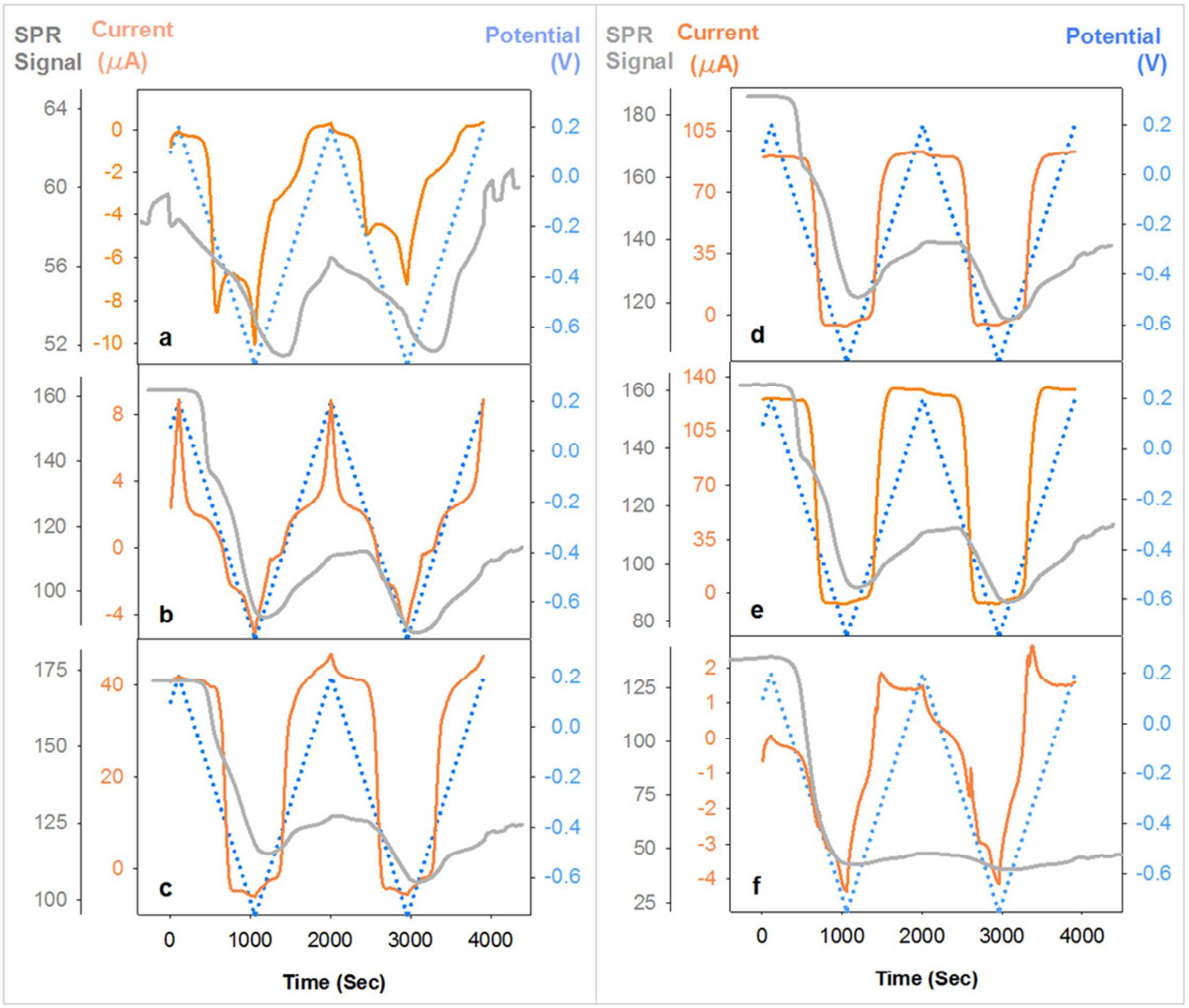

Figure 2. CVs at different growth phases depicted in Figure 1. Two CVs were performed consecutively from 0.20 V to -0.75 V vs. Ag/AgCl (0.40 to -0.55 V vs. SHE) at 1 mv/s. a) abiotic, b) lag phase, c) early growth, d) mid growth, e) stationary phase, f) non-turnover. See supplemental materials for biological replicates.

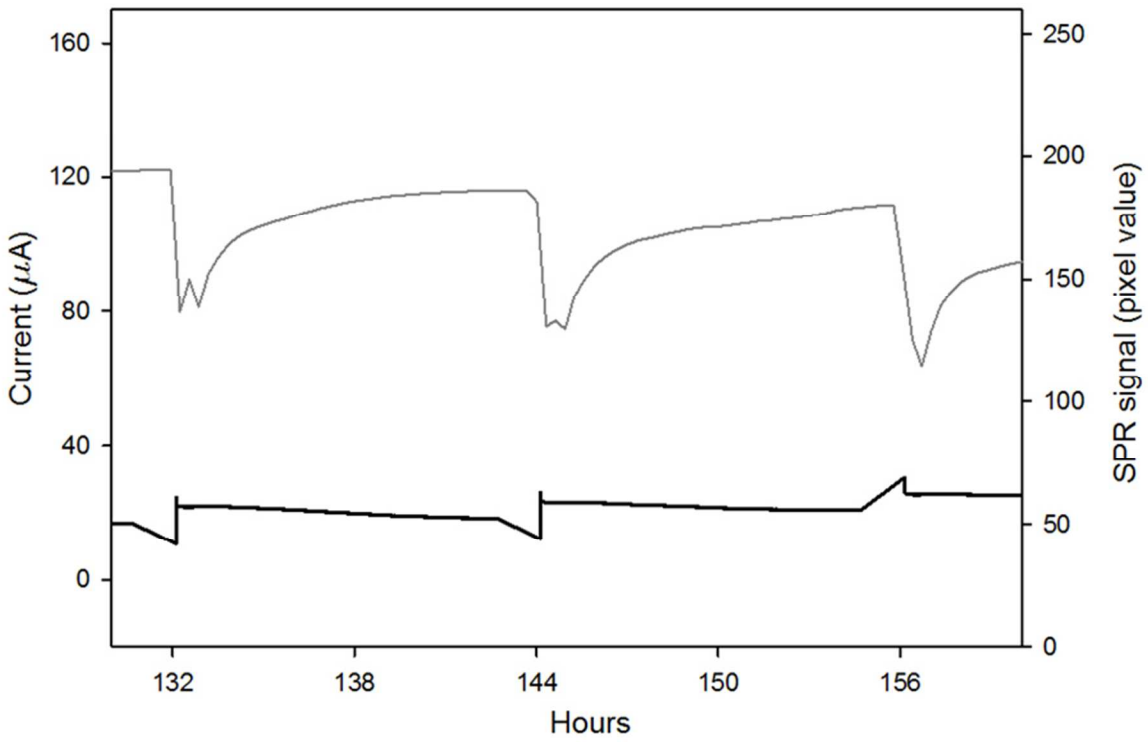

Figure 3. Representative chronoamperometry data from Figure 1 (magnified) comparing recovery of the SPR signal (gray) to turnover current (black) after performing two consecutive CVs at 132 h, 144 h and 156 h. Turnover current (recovers almost immediately whereas the SPR signal takes as long as 12 hours to recover.

References

1. Yates, M. D.; Eddie, B. J.; Lebedev, N.; Kotloski, N. J.; Strycharz-Glaven, S. M.; Tender, L. M., On the relationship between long-distance and heterogeneous electron transfer in electrode-grown Geobacter sulfurreducens biofilms. *Bioelectrochemistry* **2018,** *119* (Supplement C), 111-118.
2. Zacharoff, L.; Chan, C. H.; Bond, D. R., Reduction of low potential electron acceptors requires the CbcL inner membrane cytochrome of Geobacter sulfurreducens. *Bioelectrochemistry* **2016,** *107*, 7-13.
3. Levar, C. E.; Hoffman, C. L.; Dunshee, A. J.; Toner, B. M.; Bond, D. R., Redox potential as a master variable controlling pathways of metal reduction by Geobacter sulfurreducens. *ISME J* **2017,** *11* (3), 741-752.
4. Gralnick, J. A.; Newman, D. K., Extracellular respiration. *Mol. Microbiol.* **2007,** *65* (1), 1-11.
5. Zhang, X.; Philips, J.; Roume, H.; Guo, K.; Rabaey, K.; Prévoteau, A., Rapid and Quantitative Assessment of Redox Conduction Across Electroactive Biofilms by using Double Potential Step Chronoamperometry. *ChemElectroChem* **2017,** *4* (5), 1026-1036.
6. Steidl, R. J.; Lampa-Pastirk, S.; Reguera, G., Mechanistic stratification in electroactive biofilms of Geobacter sulfurreducens mediated by pilus nanowires. *Nat Commun* **2016,** *7*, 12217.
7. Lovley, D. R., Electromicrobiology. *Annu Rev Microbiol* **2012,** *66* (1), 391-409.
8. Yates, M. D.; Eddie, B. J.; Kotloski, N. J.; Lebedev, N.; Malanoski, A. P.; Lin, B. C.; Strycharz-Glaven, S. M.; Tender, L. M., Toward understanding long-distance extracellular electron transport in an electroautotrophic microbial community. *Energy & Environmental Science* **2016,** *9* (11), 3544-3558.
9. Schroder, U., Anodic electron transfer mechanisms in microbial fuel cells and their energy efficiency. *Physical Chemistry Chemical Physics* **2007,** *9* (21), 2619-2629.
10. TerAvest, M. A.; Ajo-Franklin, C. M., Transforming exoelectrogens for biotechnology using synthetic biology. *Biotechnol Bioeng* **2016,** *113* (4), 687-97.
11. Tender, L. M.; Reimers, C. E.; Stecher, H. A., 3rd; Holmes, D. E.; Bond, D. R.; Lowy, D. A.; Pilobello, K.; Fertig, S. J.; Lovley, D. R., Harnessing microbially generated power on the seafloor. *Nature Biotechnology* **2002,** *20* (8), 821-5.
12. Bond, D. R.; Holmes, D. E.; Tender, L. M.; Lovely, D. R., Electrode-reducing microorganisms that harvest energy from marine sediments. *Science* **2002,** *295*, 483-485.
13. Zhang, S.; You, J.; An, N.; Zhao, J.; Wang, L.; Cheng, Z.; Ye, J.; Chen, D.; Chen, J., Gaseous toluene powered microbial fuel cell: Performance, microbial community, and electron transfer pathway. *Chem Eng J* **2018,** *351*, 515-522.
14. Zhang, S. H.; You, J. P.; Kennes, C.; Cheng, Z. W.; Ye, J. X.; Chen, D. Z.; Chen, J. M.; Wang, L. D., Current advances of VOCs degradation by bioelectrochemical systems: A review. *Chem Eng J* **2018,** *334*, 2625-2637.
15. Manabe, S.; Wetherald, R. T., Thermal Equilibrium of the Atmosphere with a Given Distribution of Relative Humidity. *Journal of the Atmospheric Sciences* **1967,** *24* (3), 241-259.
16. Cox, P. M.; Betts, R. A.; Jones, C. D.; Spall, S. A.; Totterdell, I. J., Acceleration of global warming due to carbon-cycle feedbacks in a coupled climate model. *Nature* **2000,** *408*, 184.
17. Schreier, M.; Heroguel, F.; Steier, L.; Ahmad, S.; Luterbacher, J. S.; Mayer, M. T.; Luo, J. S.; Gratzel, M., Solar conversion of CO2 to CO using Earth-abundant electrocatalysts prepared by atomic layer modification of CuO. *Nat Energy* **2017,** *2* (7), 17087.
18. Marshall, C. W.; Ross, D. E.; Fichot, E. B.; Norman, R. S.; May, H. D., Long-term operation of microbial electrosynthesis systems improves acetate production by autotrophic microbiomes. *Environ Sci Technol* **2013,** *47* (11), 6023-9.
19. Marshall, C. W.; Ross, D. E.; Fichot, E. B.; Norman, R. S.; May, H. D., Electrosynthesis of commodity chemicals by an autotrophic microbial community. *Appl Environ Microbiol* **2012,** *78* (23), 8412-20.
20. Arrhenius, S., *Das Werden der Welten*. Academic Publishing House: Leipzig, 1908.

21. Guo, K.; Freguia, S.; Dennis, P. G.; Chen, X.; Donose, B. C.; Keller, J.; Gooding, J. J.; Rabaey, K., Effects of Surface Charge and Hydrophobicity on Anodic Biofilm Formation, Community Composition, and Current Generation in Bioelectrochemical Systems. *Environmental Science & Technology* **2013,** *47* (13), 7563-7570.
22. LaBelle, E., Bond, D. R. , Cyclic voltammetry of electrode-attached bacteria. In *Bioelectrochemical systems : from extracellular electron transfer to biotechnological application*, Rabaey, K., Ed. IWA Publishing: London; New York, 2011.
23. Strycharz, S. M.; Malanoski, A. P.; Snider, R. M.; Yi, H.; Lovley, D. R.; Tender, L. M., Application of cyclic voltammetry to investigate enhanced catalytic current generation by biofilm-modified anodes of Geobacter sulfurreducens strain DL1 vs. variant strain KN400. *Energ Environ Sci* **2011,** *4* (3), 896-913.
24. Torres, C. I.; Marcus, A. K.; Parameswaran, P.; Rittmann, B. E., Kinetic experiments for evaluating the Nernst-Monod model for anode-respiring bacteria (ARB) in a biofilm anode. *Environmental Science & Technology* **2008,** *42* (17), 6593-6597.
25. Strycharz-Glaven, S. M.; Tender, L. M., Study of the mechanism of catalytic activity of G. sulfurreducens biofilm anodes during biofilm growth. *ChemSusChem* **2012,** *5* (6), 1106-1118.
26. Gregoire, K. P.; Glaven, S. M.; Hervey, J.; Lin, B. C.; Tender, L. M., Enrichment of a High-Current Density Denitrifying Microbial Biocathode. *J. Electrochem. Soc.* **2014,** *161* (13), H3049-H3057.
27. Zhang, X.; Philips, J.; Roume, H.; Guo, K.; Rabaey, K.; Prevoteau, A., Rapid and Quantitative Assessment of Redox Conduction Across Electroactive Biofilms by using Double Potential Step Chronoamperometry. *Chemelectrochem* **2017,** *4* (5), 1026-1036.
28. Yates, M. D.; Strycharz-Glaven, S. M.; Golden, J. P.; Roy, J.; Tsoi, S.; Erickson, J. S.; El-Naggar, M. Y.; Barton, S. C.; Tender, L. M., Measuring conductivity of living Geobacter sulfurreducens biofilms. *Nature Nanotechnology* **2016,** *11* (11), 910-913.
29. Yates, M. D.; Golden, J. P.; Roy, J.; Strycharz-Glaven, S. M.; Tsoi, S.; Erickson, J. S.; El-Naggar, M. Y.; Calabrese Barton, S.; Tender, L. M., Thermally activated long range electron transport in living biofilms. *Physical Chemistry Chemical Physics* **2015,** *17* (48), 32564-32570.
30. Strycharz-Glaven, S. M.; Roy, J.; Boyd, D.; Snider, R.; Erickson, J. S.; Tender, L. M., Electron Transport through Early Exponential-Phase Anode-Grown Geobacter sulfurreducens Biofilms. *ChemElectroChem* **2014,** *1* (11), 1957-1965.
31. Snider, R. M.; Strycharz-Glaven, S. M.; Tsoi, S. D.; Erickson, J. S.; Tender, L. M., Long-range electron transport in Geobacter sulfurreducens biofilms is redox gradient-driven. *P Natl Acad Sci USA* **2012,** *109* (38), 15467-15472.
32. Strycharz-Glaven, S. M.; Snider, R. M.; Guiseppi-Elie, A.; Tender, L. M., On the electrical conductivity of microbial nanowires and biofilms. *Energy & Environmental Science* **2011,** *4*, 4366-4379.
33. Robuschi, L.; Pablo Tomba, J.; Schrott, G. D.; Sebastian Bonanni, P.; Mariela Desimone, P.; Pablo Busalmen, J., Spectroscopic Slicing to Reveal Internal Redox Gradients in Electricity-Producing Biofilms. *Angewandte Chemie-International Edition* **2013,** *52* (3), 925-928.
34. He, Z.; Mansfeld, F., Exploring the use of electrochemical impedance spectroscopy (EIS) in microbial fuel cell studies. *Energy & Environmental Science* **2009,** *2* (2), 215-219.
35. Yoho, R. A.; Popat, S. C.; Torres, C. I., Dynamic Potential-Dependent Electron Transport Pathway Shifts in Anode Biofilms of Geobacter sulfurreducens. *Chemsuschem* **2014,** *7* (12), 3413-3419.
36. Liu, Y.; Bond, D. R., Long-distance electron transfer by G. sulfurreducens biofilms results in accumulation of reduced c-type cytochromes. *ChemSusChem* **2012,** *5* (6), 1047-1053.
37. Liu, Y.; Kim, H.; Franklin, R. R.; Bond, D. R., Linking spectral and electrochemical analysis to monitor c-type cytochrome redox status in living Geobacter sulfurreducens biofilms. *ChemPhysChem* **2011,** *12* (12), 2235-2241.
38. Bond, D. R.; Strycharz-Glaven, S. M.; Tender, L. M.; Torres, C. I., On electron transport through Geobacter biofilms. *ChemSusChem* **2012,** *5* (6), 1099-1105.
39. Lebedev, N.; Strycharz-Glaven, S. M.; Tender, L. M., High resolution AFM and single-cell resonance Raman spectroscopy of Geobacter sulfurreducens biofilms early in growth. *Frontiers in Energy Research* **2014,** *2*, 34.

40. Lebedev, N.; Strycharz-Glaven, S. M.; Tender, L. M., Spatially Resolved Confocal Resonant Raman Microscopic Analysis of Anode-Grown Geobacter sulfurreducens Biofilms. *ChemPhysChem* **2014,** *15* (2), 320-327.
41. Virdis, B.; Harnisch, F.; Batstone, D. J.; Rabaey, K.; Donose, B. C., Non-invasive characterization of electrochemically active microbial biofilms using confocal Raman microscopy. *Energy & Environmental Science* **2012,** *5* (5), 7017-7024.
42. Millo, D.; Harnisch, F.; Patil, S. A.; Ly, H. K.; Schroder, U.; Hildebrandt, P., In Situ Spectroelectrochemical Investigation of Electrocatalytic Microbial Biofilms by Surface-Enhanced Resonance Raman Spectroscopy. *Angewandte Chemie-International Edition* **2011,** *50* (11), 2625-2627.
43. Ly, H. K.; Harnisch, F.; Hong, S. F.; Schroder, U.; Hildebrandt, P.; Millo, D., Unraveling the Interfacial Electron Transfer Dynamics of Electroactive Microbial Biofilms Using Surface-Enhanced Raman Spectroscopy. *Chemsuschem* **2013,** *6* (3), 487-492.
44. Schmidt, I.; Pieper, A.; Wichmann, H.; Bunk, B.; Huber, K.; Overmann, J.; Walla, P. J.; Schroeder, U., In Situ Autofluorescence Spectroelectrochemistry for the Study of Microbial Extracellular Electron Transfer. *Chemelectrochem* **2017,** *4* (10), 2515-2519.
45. Kubannek, F.; Schroder, U.; Krewer, U., Revealing metabolic storage processes in electrode respiring bacteria by differential electrochemical mass spectrometry. *Bioelectrochemistry* **2018,** *121*, 160-168.
46. Shan, X. N.; Patel, U.; Wang, S. P.; Iglesias, R.; Tao, N. J., Imaging Local Electrochemical Current via Surface Plasmon Resonance. *Science* **2010,** *327* (5971), 1363-1366.
47. Homola, J.; Yee, S. S.; Gauglitz, G., Surface plasmon resonance sensors: review. *Sensor Actuat B-Chem* **1999,** *54* (1-2), 3-15.
48. O'Brien, M. J., II; Brueck, S. R. J.; Perez-Luna, V. H.; Tender, L. M.; Lopez, G. P., SPR biosensors: Simultaneously removing thermal and bulk-composition effects. *Biosensors and Bioelectronics* **1999,** *14* (2), 145-154.
49. Nelson, B. P.; Grimsrud, T. E.; Liles, M. R.; Goodman, R. M.; Corn, R. M., Surface plasmon resonance imaging measurements of DNA and RNA hybridization adsorption onto DNA microarrays. *Anal Chem* **2001,** *73* (1), 1-7.
50. Arima, Y.; Iwata, H., Effect of wettability and surface functional groups on protein adsorption and cell adhesion using well-defined mixed self-assembled monolayers. *Biomaterials* **2007,** *28* (20), 3074-3082.
51. Walper, S. A.; Lee, P. A. B.; Goldman, E. R.; Anderson, G. P., Comparison of single domain antibody immobilization strategies evaluated by surface plasmon resonance. *Journal of Immunological Methods* **2013,** *388* (1-2), 68-77.
52. Wang, S.; Huang, X.; Shan, X.; Foley, K. J.; Tao, N., Electrochemical Surface Plasmon Resonance: Basic Formalism and Experimental Validation. *Anal Chem* **2010,** *82* (3), 935-941.
53. Iwasaki, Y.; Horiuchi, T.; Morita, M.; Niwa, O., Electrochemical reaction of Fe (CN)(6)(3-)/(4-) on gold electrodes analyzed by surface plasmon resonance. *Surf. Sci.* **1999,** *427-28*, 195-198.
54. Iwasaki, Y.; Horiuchi, T.; Niwa, O., Detection of electrochemical enzymatic reactions by surface plasmon resonance measurement. *Anal Chem* **2001,** *73* (7), 1595-1598.
55. Boussaad, S.; Pean, J.; Tao, N. J., High-resolution multiwavelength surface plasmon resonance spectroscopy for probing conformational and electronic changes in redox proteins. *Anal Chem* **2000,** *72* (1), 222-226.
56. Wang, Y.; Wang, H.; Chen, Y. H.; Wang, Y. X.; Chen, H. Y.; Shan, X. N.; Tao, N. J., Fast Electrochemical and Plasmonic Detection Reveals Multitime Scale Conformational Gating of Electron Transfer in Cytochrome c. *J Am Chem Soc* **2017,** *139* (21), 7244-7249.
57. Zacharoff, L. A.; Morrone, D. J.; Bond, D. R., Geobacter sulfurreducens Extracellular Multiheme Cytochrome PgcA Facilitates Respiration to Fe(III) Oxides But Not Electrodes. *Front Microbiol* **2017,** *8*.
58. Chan, C. H.; Levar, C. E.; Jimenez-Otero, F.; Bond, D. R., Genome Scale Mutational Analysis of Geobacter sulfurreducens Reveals Distinct Molecular Mechanisms for Respiration and Sensing of Poised Electrodes versus Fe(III) Oxides. *J Bacteriol* **2017,** *199* (19).

59. Liu, Y. M.; Wang, Z. M.; Liu, J.; Levar, C.; Edwards, M. J.; Babauta, J. T.; Kennedy, D. W.; Shi, Z.; Beyenal, H.; Bond, D. R.; Clarke, T. A.; Butt, J. N.; Richardson, D. J.; Rosso, K. M.; Zachara, J. M.; Fredrickson, J. K.; Shi, L., A trans-outer membrane porin-cytochrome protein complex for extracellular electron transfer by Geobacter sulfurreducens PCA. *Env Microbiol Rep* **2014,** *6* (6), 776-785.
60. Levar, C. E.; Chan, C. H.; Mehta-Kolte, M. G.; Bond, D. R., An Inner Membrane Cytochrome Required Only for Reduction of High Redox Potential Extracellular Electron Acceptors. *Mbio* **2014,** *5* (6).
61. Richter, H.; Nevin, K. P.; Jia, H. F.; Lowy, D. A.; Lovley, D. R.; Tender, L. M., Cyclic voltammetry of biofilms of wild type and mutant Geobacter sulfurreducens on fuel cell anodes indicates possible roles of OmcB, OmcZ, type IV pili, and protons in extracellular electron transfer. *Energy & Environmental Science* **2009,** *2* (5), 506-516.
62. Reguera, G., Microbial nanowires and electroactive biofilms. *FEMS Microbiology Ecology* **2018**, fiy086-fiy086.
63. Golden, J. P.; Burden, D. K.; Fears, K. P.; Barlow, D. E.; So, C. R.; Burns, J.; Miltenberg, B.; Orihuela, B.; Rittshof, D.; Spillmann, C. M.; Wahl, K. J.; Tender, L. M., Imaging Active Surface Processes in Barnacle Adhesive Interfaces. *Langmuir* **2016,** *32* (2), 541-550.
64. Wang, S.; Boussaad, S.; Wang, S.; Tao, N. J., High sensitivity stark spectroscopy obtained by surface plasmon resonance measurement. *Anal Chem* **2000,** *72* (17), 4003-4008.
65. Fang, S. P.; Lee, H. J.; Wark, A. W.; Corn, R. M., Attomole microarray detection of MicroRNAs by nanoparticle-amplified SPR imaging measurements of surface polyadenylation reactions. *J Am Chem Soc* **2006,** *128* (43), 14044-14046.
66. Smith, E. A.; Thomas, W. D.; Kiessling, L. L.; Corn, R. M., Surface plasmon resonance imaging studies of protein-carbohydrate interactions. *J Am Chem Soc* **2003,** *125* (20), 6140-6148.
67. Liu, Y.; Chin, L. K.; Ser, W.; Ayi, T. C.; Ho, W. M.; Yap, P. H.; Leprince-Wang, Y.; Bourouina, T. In *A SINGLE LIVING BACTERIUM'S REFRACTIVE INDEX MEASUREMENT BY USING OPTOFLUIDIC IMMERSION REFRACTOMETRY* 17th International Conference on Miniaturized Systems for Chemistry and Life Sciences, Freiburg, Germany, Freiburg, Germany, 2013; pp 263-265.
68. Phan, H.; Yates, M. D.; Kirchhofer, N. D.; Bazan, G. C.; Tender, L. M.; Nguyen, T. Q., Biofilm as a redox conductor: a systematic study of the moisture and temperature dependence of its electrical properties. *Physical Chemistry Chemical Physics* **2016,** *18* (27), 17815-17821.
69. Filion-Cote, S.; Melaine, F.; Kirk, A. G.; Tabrizian, M., Monitoring of bacterial film formation and its breakdown with an angular-based surface plasmon resonance biosensor. *Analyst* **2017,** *142* (13), 2386-2394.
70. Wang, S. P.; Forzani, E. S.; Tao, N. J., Detection of heavy metal ions in water by high-resolution surface plasmon resonance spectroscopy combined with anodic stripping voltammetry. *Anal Chem* **2007,** *79* (12), 4427-4432.
71. Wang, S.; Boussaad, S.; Tao, N. J., Surface plasmon resonance enhanced optical absorption spectroscopy for studying molecular adsorbates. *Rev Sci Instrum* **2001,** *72* (7), 3055-3060.
72. Bard, A. J.; Faulkner, L. R., *Electrochemical Methods: Fundamentals and Applications,*. Second ed.; John Wiley & Sons, Inc: New York, 2001.
73. Smith, D. K.; Tender, L. M.; Lane, G. A.; Licht, S.; Wrighton, M. S., Chemically-Induced Release of Charge from a Rectifying Polymer Based on Viologen and Quinone Subunits. *J Am Chem Soc* **1989,** *111* (3), 1099-1105.
74. Strycharz, S. M.; Glaven, R. H.; Coppi, M. V.; Gannon, S. M.; Perpetua, L. A.; Liu, A.; Nevin, K. P.; Lovley, D. R., Gene expression and deletion analysis of mechanisms for electron transfer from electrodes to Geobacter sulfurreducens. *Bioelectrochemistry* **2011,** *80* (2), 142-150.

Graphical abstract (Table of contents)

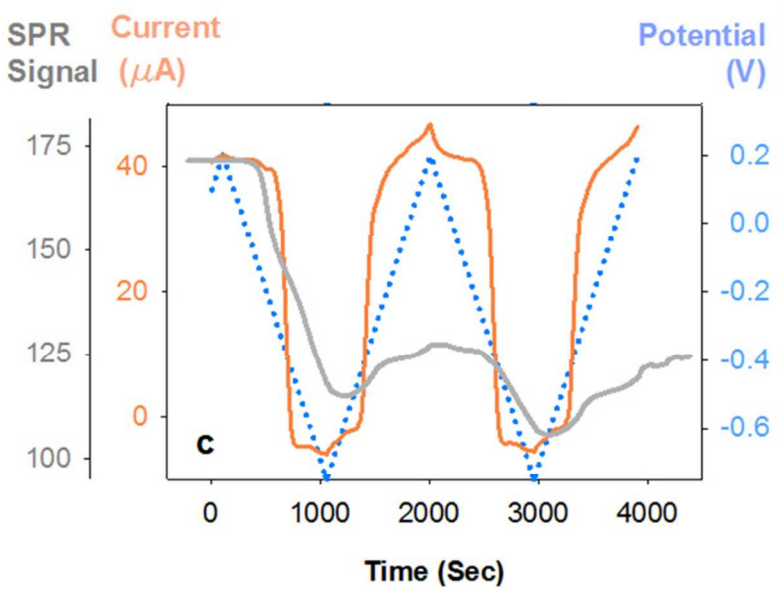

Electrochemical Surface Plasmon Resonance (ESPR) of an electrode-grown *Geobacter sulfurreducens* biofilm indicating that when the potential is swept from reducing to strongly oxidizing, as much as 70% of cytochromes residing within hundreds of nanometers from the electrode surface remain trapped in the reduced form. This does not effect on the ability of the biofilm to transfer its respired electrons to the electrode surface.